

Geophysical Research Letters



RESEARCH LETTER

10.1029/2019GL084342

Key Points:

- First successful measurements of surface nuclear magnetic resonance signal with a bipole formed by a grounded electrode pair
- Surface nuclear magnetic resonance signal measured by grounded produces the same groundwater model as conventional coincident loop sounding
- Surface NMR signals measured with bipoles and dipoles opens field for novel NMR measurements using resistivity transects

Correspondence to:

A. C. Davis,
aaron.davis@csiro.au

Citation:

Davis, A. C., Skibbe, N., & Müller-Petke, M. (2019). First measurements of surface nuclear magnetic resonance signals in a grounded bipole. *Geophysical Research Letters*, 46, 9620–9627. <https://doi.org/10.1029/2019GL084342>

Received 29 JUN 2019

Accepted 8 AUG 2019

Accepted article online 19 AUG 2019

Published online 26 AUG 2019

©2019. The Authors.

This is an open access article under the terms of the Creative Commons Attribution License, which permits use, distribution and reproduction in any medium, provided the original work is properly cited.

First Measurements of Surface Nuclear Magnetic Resonance Signals in a Grounded Bipole

A. C. Davis¹ , N. Skibbe² , and M. Müller-Petke² 

¹CSIRO Mineral Resources, Kensington, Western Australia, Australia, ²Leibniz Institute for Applied Geophysics, Hannover, Germany

Abstract Surface nuclear magnetic resonance (surface NMR) soundings are geophysical techniques that offer direct detection of groundwater. Ordinary surface NMR soundings are achieved with a wire loop that acts as both transmitter and receiver. We extend the capability of the technique by using a grounded electrical bipole as the measurement sensor. We provide the first successful measurements of surface NMR signals taken with a grounded electrode pair on a beach outside Perth, Western Australia. Simple changes to existing equations are sufficient to provide forward models for the changes in measurement technique, and the resulting groundwater models are consistent with coincident loop soundings. Our result opens the field for novel sounding techniques of surface NMR signals that could have broad impact on near-surface groundwater investigations.

Plain Language Summary Surface nuclear magnetic resonance (surface NMR) is a geophysical technique that can directly measure the presence of water in the subsurface. An NMR sounding typically uses a large loop to generate a pulse that excites water into a higher energy level. As the water relaxes back to the equilibrium state, it releases energy that can be detected in the loop. Bipoles are often used in geophysics to determine the ground's electrical structure. Our work uses bipoles to measure groundwater. This has the advantage that the bipoles could be used for both resistivity sounding and surface NMR measurements in the same deployment. We have successfully measured surface NMR signals using a bipole at a beach near Perth, Western Australia. We used a closed loop as the transmitter, and the electrodes were steel pegs. The signals we recorded can only be explained by the presence of groundwater. The groundwater models generated from the bipole data are consistent with models from the traditional technique. Our measurements are the first demonstration that bipoles can be used to detect water in the subsurface. This has the potential to open up an entirely new technique for groundwater detection and exploration.

1. Introduction

Surface nuclear magnetic resonance (surface NMR) is the only remote sensing geophysical technique capable of directly measuring groundwater (Behroozmand et al., 2015). The principles of operation are similar to those of traditional NMR whereby a transient electromagnetic pulse is employed to elevate hydrogen nuclei into an excited state, and a secondary field is generated from the relaxation of same atoms into their equilibrium. In the case of surface NMR, the secondary response provides information about the quantity and distribution of water in the subsurface. The amplitude of the secondary field is related to groundwater quantity, while the rates of decay of the field are related to pore size distribution and availability of groundwater for production.

The stationary field employed in surface NMR is provided by the geomagnetic field of the Earth, and the excitation field is generated by driving current through a closed loop. In a conventional groundwater sounding, a large surface loop is deployed to act as both transmitter of the excitation field and receiver of the secondary field (Schirov et al., 1991). Exploration depths for surface NMR are governed by changing the pulse moment of the excitation pulse (altering either the pulse duration or the peak current). Exploration is achievable to depths of about 100 m, depending on the electrical conductivity of the ground, geometry of the excitation and receiver loops, and amount of current available for the excitation pulse. A groundwater sounding is achieved by taking multiple measurements of secondary fields generated from a suite of transmission pulses

with varying pulse moments. An inversion algorithm is then required to determine a groundwater model that is consistent with the measured data (e.g., Müller-Petke & Yaramanci, 2010).

In this paper, we measure the free induction decay (FID) of surface NMR signals generated by a single excitation pulse at the Larmor frequency (determined by the Earth magnetic field). FID decays are simplest since they only require a measurement of the voltage induced in the loop by the decay of the secondary field to back to equilibrium. Estimates of the T_2^* relaxation times characteristic of FID decays are obtained by fitting a sum of exponentially decaying sinusoids to the secondary voltage for all pulse moment measurements in the sounding. Because induced voltages due to the secondary field of the surface NMR responses are typically very small relative to anthropogenic and environmental noise, many measurement repetitions are necessary in a single sounding. Consequently, even simple T_2^* measurements can take hours to perform.

A 1-D surface NMR sounding typically involves a single surface loop that functions as both transmitter and receiver. However, surface NMR can also be used to produce 2-D and 3-D groundwater images by employing multiple loops. For a 2-D sounding, one must employ several loops that act as transmitters and as receivers (Hertrich et al., 2009). Alternatively, the transmitter can be deployed as an elongated loop with several receiver loops deployed along the total length (Jiang et al., 2014). In both cases, a great deal of wire needs to be deployed for the multiple-loop deployment, adding significantly to time spent in the field. Simplifications to surface NMR measurements can be made. For example, Davis et al. (2014) used a SQUID sensor in an attempt to reduce receiver size. However, SQUIDS are expensive devices to acquire and use. In the present work, we propose the use of a grounded electrical bipole to take measurements of surface NMR signals. Grounded electrodes are easy to deploy in the field and are routinely used to measure electrical resistivity, knowledge of which is fundamental to accurate modeling of surface NMR (Braun et al., 2005; Grombacher et al., 2019; Irons & Li, 2014; Shushakov, 1996; Weichman et al., 2000). We present the first successful measurement of surface NMR signals using a closed-loop transmitter and grounded electrodes as the receiver. We demonstrate that signals measured in the grounded bipole may be explained as arriving from a groundwater model that is consistent for both bipole and coincident loop geometry.

2. Measurement

2.1. Location

In order to demonstrate the feasibility of measuring a surface NMR signal with a bipole pair, we chose a measurement site on the shore of the Indian Ocean. A popular location north of Perth, The Spot surf beach is close to the suburb of Two Rocks, Western Australia. The area is composed of Becher and Safety Bay sands overlying Tamala Limestone formations (Smith et al., 2011). Tamala Limestone deposits, which are commonly found along the coastline of the entire Perth Basin, are formed from coastal quartzite sand dunes mixed with aeolian shell fragments. Sedimentation and lithification occurred from mid-Pleistocene to early Holocene. The karstic limestone formations are of varying density and porosity, mainly due to weathering and erosive processes. The Spot beach is reached by a short descent from the car park along a sand track that has outcrops of vuggy limestone. The same outcrops are responsible for the surf waves offshore. Our experiment was situated on the beach sands surrounded by bluffs of Tamala Limestone. The sand was dry to a depth of about 0.5 m.

2.2. Description of Measurement

For closed-loop transmission and recording of all NMR signals, we used the Vista-Clara GMR surface nuclear magnetic resonance equipment (Vista Clara Inc. 2019). The beach was not large, allowing us to place only a 30 × 30-m square loop on the flat section. The loop was aligned to be parallel and perpendicular to magnetic North. A bipole was constructed using two bundles of six stainless steel resistivity pegs that were connected via wires to the Channel 3 receiver port of the GMR device. The poles of the bipole pair were separated by 50 m along magnetic north and bisecting the transmitter loop. The wires connecting the grounded bipole met in the center of the loop and then were paired back to the GMR so that the experimental setup resembled the drawing in Figure 1. A remote noise coil was deployed to the north of the loop (Walsh, 2008), was found to contain surface NMR signal, and was not used in processing.

The International Geomagnetic Reference Field model (Thébault et al., 2015) for The Spot on the day we made our measurement calculated a total magnetic field of 57873.46 nT with a declination of -65.68° , which equated to an estimated Larmor frequency of $f_L = 2464.1$ Hz for hydrogen atoms. Measurements were made

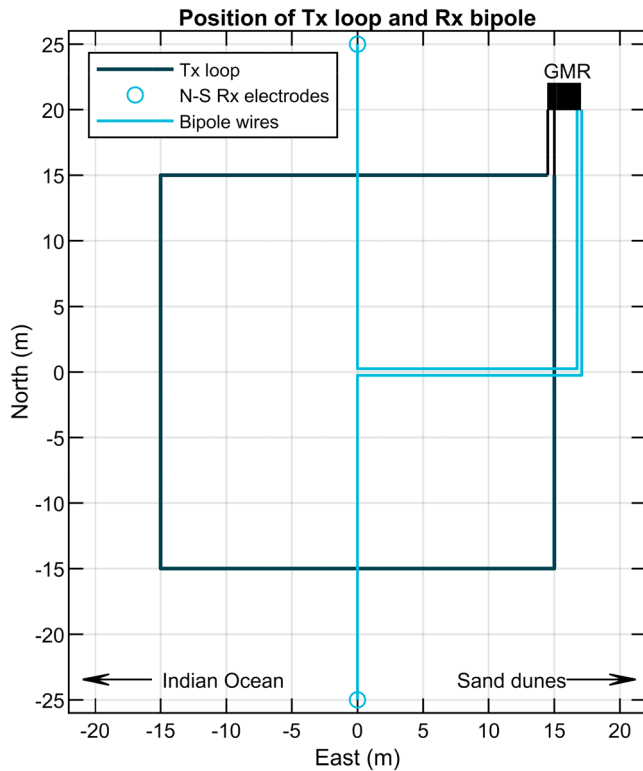


Figure 1. Layout of transmitter loop (square) and receiver bipole locations. Electrode positions are marked with open circles, and connection wire shown with blue lines.

using an FID sequence with pulse duration of 20 ms; 20 pulses were used with pulse moments logarithmically spaced between 0.2486 and 5.0199 As. We collected 18 stacks of each pulse, amounting to 360 records. Signal was collected simultaneously both in the coincident loop and across the bipole.

2.3. Processing and Spectral Analysis

Prior to stacking the pulse moments for noise reduction, we processed individual records for sferic activity and 50-Hz power line coupling noise. Broadband noise from lightning strike was detected and eliminated from the data in a two-part process. First, we used the nonlinear energy operator to detect and remove spikes in the raw data following Dalgaard et al. (2012). Power line frequencies are estimated by a model-based approach similar to (Larsen et al., 2013), and constructing a notch filter over the first 80 or so harmonics. Once the power line signal is removed, the nonlinear energy operator filter is applied again to remove the remaining sferics. We filtered the time series data using a band-pass filter of 500-Hz width centered at our expected Larmor frequency. Finally, each pulse moment record was stacked to create 40 time series recordings (20 pulse moment stacks, recorded in the coincident loop and bipole).

We estimated the surface NMR signal from the FID data using a Bayesian spectral analysis first developed by Bretthorst (1988). The method uses probability theory to simultaneously predict Larmor frequency f_L , a single T_2^* characteristic decay time, and the in-phase and quadrature amplitudes of the surface NMR signal from a noisy time series. Since an FID response is expected to be present in most records from the sounding experiment, the estimation of the surface NMR signal is calculated for all 40 records simultaneously assuming a common f_L and T_2^* . Our process uses the Nelder-Mead simplex method to maximize the probability func-

tion (Lagarias et al., 1998). We found that $f_L = 2468.5$ Hz and $T_2^* = 563$ ms for all records. Variance of the amplitudes is predicted as well, based on the supplied noise model. Figure 2a shows an example of a surface NMR signal in a time series for a single stacked pulse moment measured in the north-south bipole. The processed time series is shown in black, and the estimated signal for the 0.6229 As pulse moment record is shown in blue. Panel (b) shows the amplitude spectrum of the measured and predicted data. The in-phase and quadrature amplitudes are estimated to be $A_r = -88 \pm 6$ nV and $A_q = 14 \pm 6$ nV, respectively. The signal to noise ratio of the surface NMR FID decay for this pulse moment is only 0.61; however, the probability odds ratio of the surface NMR signal to the best fitting sine wave of the same frequency is e^{1161} :1, which is a practical certainty that we have detected a FID surface NMR signal across the grounded electrodes (see for a description of log-odds ratios; Gregory, 2010). The complete set of estimated amplitudes, for both the coincident loop and the grounded electrode measurements, is shown in Figures 4a and 4b.

3. Forward Modeling

The surface NMR voltage that is predicted to be induced in a receiver as a consequence of FID of hydrogen nuclei during a sounding experiment is described in equation 2.35 of Weichman et al. (2000). We repeat it here for completeness, mentioning only that the vectors with subscripts T and R refer to the transmitter and receiver magnetic fields, respectively:

$$V(q) = - \frac{\omega_L \gamma^2 \hbar^2 S(S+1) B_0}{3k_B T} \int d^3 r |B_R^{0\perp}(\mathbf{r})| n_N(\mathbf{r}) \times \sin \left[\frac{1}{2} \gamma q |B_T^{0\perp}(\mathbf{r})| \right] \{ \hat{\mathbf{b}}_R^0(\mathbf{r}) \cdot \hat{\mathbf{b}}_T^0(\mathbf{r}) + i \hat{\mathbf{B}}_0 \cdot [\hat{\mathbf{b}}_R^0 \times \hat{\mathbf{b}}_T^0] \}. \quad (1)$$

Equation (1) simplifies when the receiver loop is coincident with the transmitter loop (i.e., a traditional surface NMR experiment). When measuring signals with grounded electrodes, one normally thinks of current

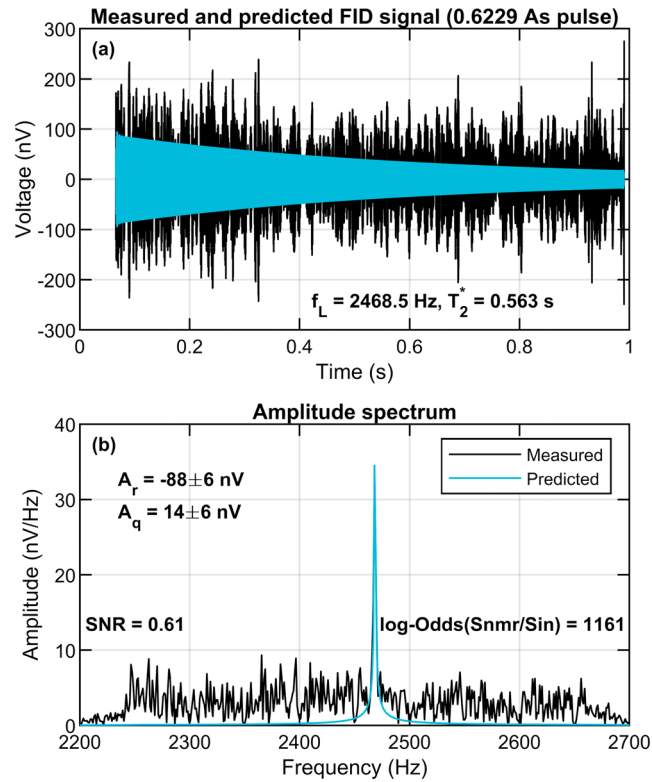


Figure 2. (a) Measured and predicted SNMR signal in the N-S bipole for the 0.6229 As stacked pulse moment. Larmor frequency (f_L) is estimated to be 2468.5 Hz, with a single exponential decay constant of 563 ms. (b) Measured and predicted amplitude spectrum for the signals in (a) showing a clear peak at the Larmor frequency. Signal-to-noise ratio of the SNMR signal is 0.61. The odds ratio of the SNMR signal to a constant sine wave at f_L is e^{1161} :1. SNMR = surface nuclear magnetic resonance; FID = free induction decay.

lines and equipotential surfaces from a direct current injection bipole. However, the theories of electromagnetics apply to bipole measurement when a time-varying primary field (from whatever source) is used to excite the subsurface. A time-varying electromagnetic field induces currents to flow in the ground which, in turn, generate secondary electromagnetic fields. This means that grounded bipoles can be used to measure magnetic fields in the subsurface. Therefore, we substitute the closed-loop receiver magnetic field terms ($B_R^{0,1}$ and $\hat{\mathbf{b}}_R^0$) of equation (1) with magnetic fields calculated from grounded electrodes with the proper geometry and subsurface electrical conductivity taken into account. We note, however, that a closed physical derivation may be necessary to prove our assumption. Since the Larmor frequency of the received surface NMR is not expected to be the same as the transmitted field, we must account for the effective fields that arise due to the 4.4 Hz off-resonance excitation of the hydrogen nuclei (Walbrecker et al., 2009).

For a one-dimensional Earth, equation (1) can be simplified by computing the integral in two dimensions and discretizing the z axis (depth) component. We expect the signal to be complex but wish to calculate using only amplitudes. The total initial-amplitude voltages from the measured FID signals can be expressed in matrix form as

$$\mathbf{d}(\mathbf{m}) = ((\mathbf{G}_r \cdot \mathbf{m})^2 + (\mathbf{G}_q \cdot \mathbf{m})^2)^{1/2}, \quad (2)$$

where $\mathbf{d}(\mathbf{m})$ is the vector of predicted amplitudes for a given set of pulse moments, \mathbf{m} is the discretized groundwater fraction model (Weichman et al., 2000, have it as $n_N(\mathbf{r})$ in equation (1)), and $\mathbf{G}_r, \mathbf{G}_q$ are the in-phase and quadrature kernel functions that encompass the physics of the surface NMR signal. We note that equation (2) is no longer linear and must be solved iteratively for a groundwater model.

To generate the kernel functions for both of the measurement configurations, all magnetic fields were calculated using Leroi, a package of the AMIRA P223 suite of EM modeling codes (Raiche et al., 2007). Leroi can be used to calculate magnetic fields in the subsurface for almost any type of electromagnetic

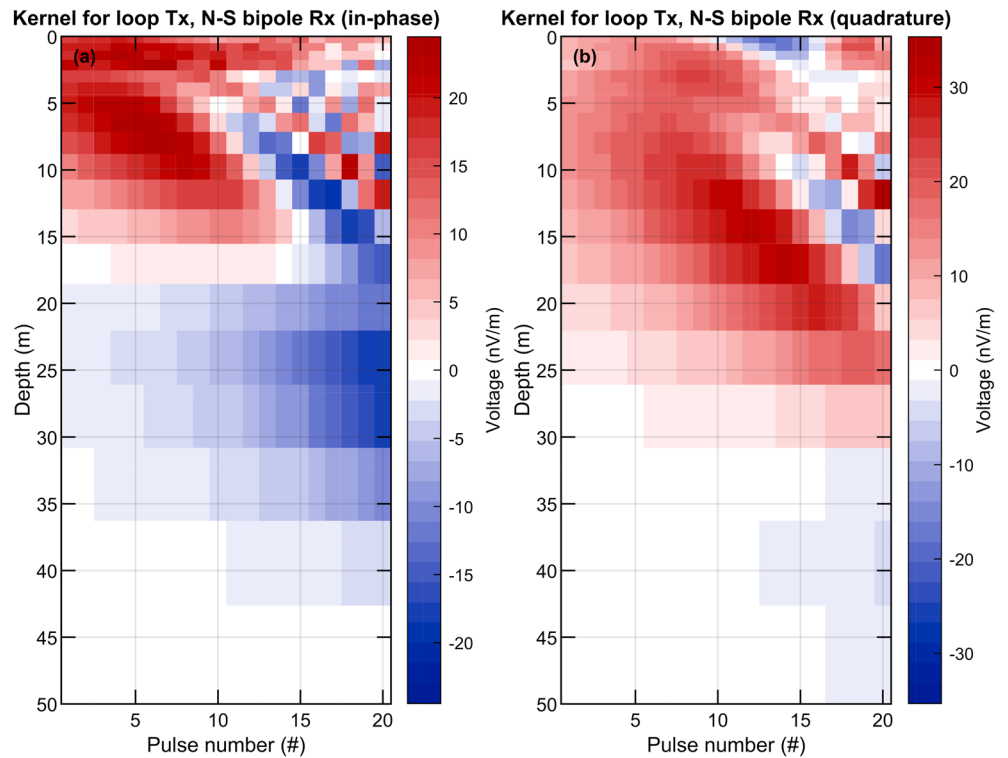


Figure 3. In-phase (a) and quadrature (b) kernel matrices for generating predicted FID voltages from groundwater models calculated using the closed rectangular loop as transmitter and the north-south grounded electrode bipole as receiver. Electrical conductivity was measured using a time domain electromagnetic sounding (Figure 4d).

configuration. We calculated magnetic fields in the subsurface due to the square transmitter and the bipole receiver. When possible, we exploited the symmetry available from the experimental setup. For the bipole receiver, the connecting wires were paired at the center of the loop and fed back to the GMR in parallel. The ground was discretized vertically using logarithmically increasing layer thickness across 20 layers with a first layer thickness of 0.4 m increasing downwards to a depth of 50 m. Electrical conductivity of the ground was measured using a 20×20 -m square central-loop time domain electromagnetic sounding (see Figure 4d). Integrations over x and y were computed numerically, yielding two different complex kernel matrices with variation in the z direction. The in-phase and quadrature kernel matrices for the square loop transmitter and the north-south bipole combination are shown in Figure 3.

4. Inversion

Equation (2) demonstrates how to predict FID voltages in the receivers for an arbitrary groundwater model. Since we already have a measured set of FID amplitudes, we need to produce a groundwater model such that the misfit between the predicted and measured data is a minimum subject to a some constraints. Specifically, we seek to explore the misfit function $F(\mathbf{m})$

$$F(\mathbf{m}) = \chi^2(\mathbf{m}), \quad (3)$$

where

$$\chi^2(\mathbf{m}) = (\mathbf{d} - \mathbf{d}(\mathbf{m}))^T \mathbf{C}_d^{-1} (\mathbf{d} - \mathbf{d}(\mathbf{m})). \quad (4)$$

In these equations, \mathbf{d} is the vector of estimated complex FID amplitudes for each pulse moment, $\mathbf{d}(\mathbf{m})$ is the forward model function for groundwater model \mathbf{m} , and \mathbf{C}_d^{-1} is the inverse data covariance matrix (assumed to be diagonal with values governed from the parameter estimation output in section 2.3).

To estimate the groundwater content of the subsurface, we use a Monte Carlo method similar to that employed by Legchenko et al. (2017). At each cycle of the Monte Carlo estimation, we randomly perturb the

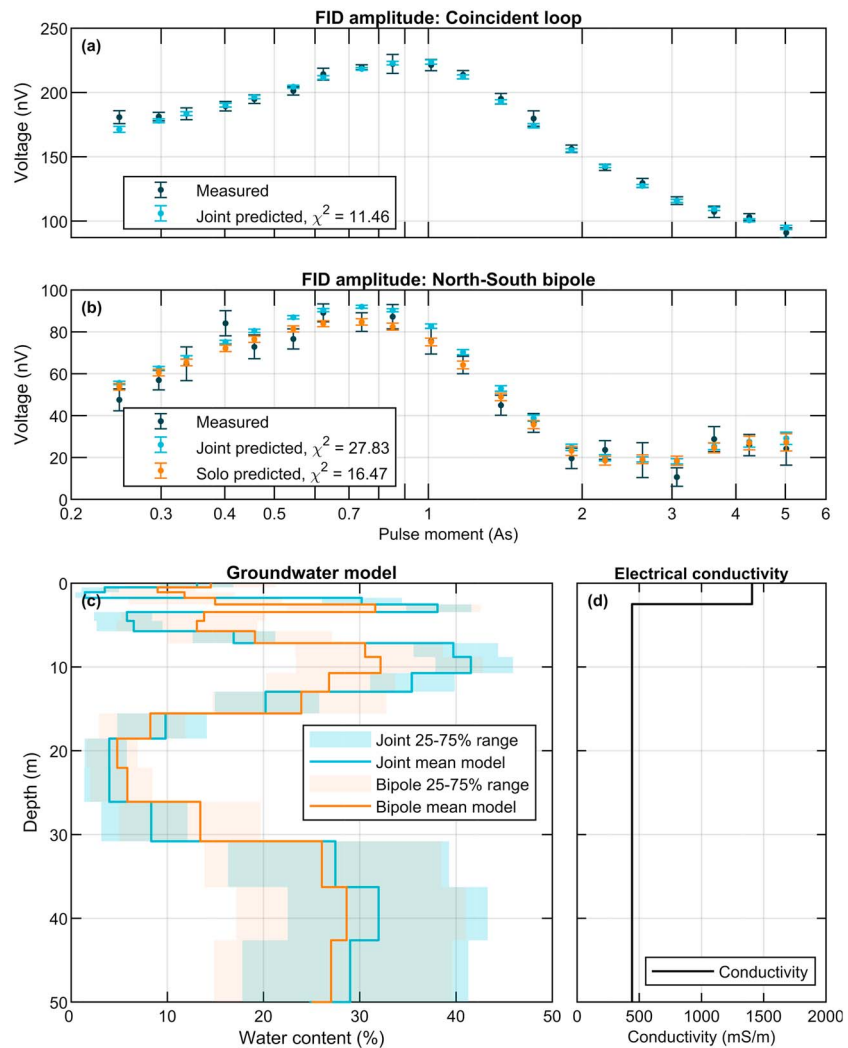


Figure 4. Free induction decay measurement and inversion results for the coincident loop and grounded bipole experiment. (a) Coincident loop. Measured amplitudes are shown with error bars. The mean posterior model is shown in light blue. (b) Grounded electrodes. Also included in (b) is the mean posterior model for the bipole electrode experiment alone. (c) Shows the mean and 25% to 75% groundwater models for the joint and bipole Monte Carlo simulations. (d) Electrical conductivity-depth model from an electromagnetic sounding. FID = free induction decay.

water content of each of the 20 layers in the groundwater model \mathbf{m} with acceptance probability

$$\alpha = \min \left\{ 1 \wedge \frac{\chi^2(\mathbf{m}_c)}{\chi^2(\mathbf{m}_p)} \right\}, \quad (5)$$

where $\chi^2(\mathbf{m}_c)$ is the misfit of the current groundwater model and $\chi^2(\mathbf{m}_p)$ is the misfit of the proposed model with water content perturbed in some layer. The proposed model is accepted if α is greater than 1, or with a probability determined by the ratio in equation (5) otherwise. Our prior range for water content for each layer is a uniform distribution between 0 and 0.5. At each step, we perturb the groundwater in a given layer with a Gaussian perturbation with a standard deviation of 0.05. The order of perturbation of the 20 layers is random for each cycle, and the cycles are repeated about 12×10^6 times. We then collect the results of the estimation, downsampled by a factor of 4. The collated results of a groundwater estimation for the joint experiment (coincident loop and bipole), and for an estimation based on the bipole alone, are shown in Figure 4. Panel (a) shows the coincident loop FID amplitudes (dark dots with error bars) and the estimated FID amplitudes for the posterior mean model of our Monte Carlo trial using both the coincident loop and bipoles as input data. The mean groundwater parameter estimation model is shown with light blue dots

and error bars. Panel (b) shows the same results, but for the grounded electrodes. Also included in (b) is the mean posterior model for the bipole electrode experiment inverted alone.

Figure 4c shows the posterior mean and 25% to 75% range groundwater models for the joint and bipole Monte Carlo simulations. An electrical conductivity-depth model from an electromagnetic sounding is shown in panel (d).

5. Discussion

Figure 2 demonstrates success at measuring surface NMR signals across the electrodes of a grounded wire. The transmitter used to generate the excitation fields in our experimental setup was a closed loop placed on the beach, guaranteeing the presence of water in the subsurface. We clearly see a peak in the amplitude spectrum at a frequency that is close to the expected Larmor frequency for the location. The surface NMR signal across the bipole can only be due to the presence of water. As we show in the figure, the odds of the signal being an exponentially damped sinusoid with Larmor frequency 2468.5 Hz are overwhelming. Since the decay time of the signal is on the order of a half a second, it must arise from subsurface water and not free water from the Indian Ocean (although this would be expected to contribute somewhat to the overall signal). Even though we admit that estimating a single characteristic decay time for the entire collection of surface NMR records does not lead to good hydrological evaluation of the pore geometry (Müller-Petke & Yaramanci, 2010), we still achieve a reasonable groundwater model with the bipole results.

Figure 3 displays the kernel matrices for the closed-loop transmitter and grounded wire receiver that we calculated with simple modifications to the derivations of Weichman et al. (2000). The complex kernel functions are used to calculate the zero-time FID amplitudes from a given groundwater model \mathbf{m} . This provides the basis for determining plausible groundwater models that can consistently fit the measured data.

We used a method to explore the groundwater model space to create ensembles of models that describe possible distributions of water in the subsurface. The mean posterior result for a joint parameter estimation for data from the coincident loop and bipole is shown in Figure 4c (blue curve). The ranges of amplitudes for the model ensembles are displayed in panels (a) and (b).

For the joint groundwater model in Figure 4c, we see an increase in water content to 3.5 m, which corresponds to seawater penetrating into the beach sands, increasing in saturation with depth. Beneath 3.5 m, we see a layer of low groundwater content which may correspond to more competent Tamala Limestone. At about 7 m the groundwater content increases again, indicating water in either sand or more weathered limestone formations. The lower electrical conductivity value indicates that this layer may contain fresher water leading to offshore discharge. The groundwater content decreases after 15 to 30 m, suggesting less porous limestone. Beneath 30 m the models lose resolution and return to the prior distribution (uniform from 0% to 50% water content, with a mean of 25%). The orange trace in Figure 4c shows the mean posterior groundwater model of the Monte Carlo estimation using only the electrical bipole measurements. When we compare it to the joint inversion model, we see a general agreement throughout the profile. We are therefore confident that the bipole measurements are capable of producing a groundwater model that is consistent with the coincident loop measurements. Without bore data at the site, our interpretation of the groundwater models is challenging, although it is known that the Tamala Limestone varies in composition, weathering, and density and also hosts freshwater aquifers that discharge offshore.

We conducted a second field test in the Yalgorup National Park south of Perth. The location of our experimental setup was a few kilometers inland from the beach on the dry Tamala Limestone dunes at the entry to the park. In this experiment, we were unable to detect surface NMR signal in the grounded bipole—even though the coincident loop data shows clear NMR signal. This result raises obvious questions about experimental design and our understanding of the forward modeling for grounded electrodes. Other factors such as contact resistance between the grounded electrodes and the earth and geometry of design are interesting questions that should be addressed in future research.

6. Conclusion

We have demonstrated that it is possible to measure surface NMR signals across a grounded bipole. Our measurements produce groundwater models that are consistent with conventional coincident loop measurements. This opens a new field for groundwater exploration using surface NMR methods. We suggest that

grounded bipoles can be used for both transmission and reception of surface NMR fields. This could allow practitioners to complete 3-D resistivity and surface NMR soundings in the same survey without extra equipment setup, and potentially simplify measurements over variable topography. The appropriate hardware for surface NMR conducted with resistivity equipment does not yet exist and development of such hardware is required before measurements are commonplace. We would like to explore the coupling structure of bipoles to closed loops in order to optimize surface NMR bipole surveys, perhaps there are arrangements of geometry with loops and bipoles that can focus better in the near surface or more deeply. We are hopeful that our contribution will attract further research and development to the field of surface nuclear magnetic resonance studies.

Acknowledgments

A. C. D. thanks CSIRO for permission to publish. N. S. has received funds from the Deutsche Forschungsgemeinschaft (DFG) under Grant MU 3318/3-1. We thank Kevin Cahill for his assistance in the field. None of the authors have a conflict of interest with respect to the findings of this paper. Data are available from the CSIRO Data Access Portal (Davis, 2019).

References

- Bhroozmand, A. A., Keating, K., & Auken, E. (2015). A review of the principles and applications of the NMR technique for near-surface characterization. *Surveys in Geophysics*, *36*(1), 27–85.
- Braun, M., Hertrich, M., & Yaramanci, U. (2005). Study on complex inversion of magnetic resonance sounding signals. *Near Surface Geophysics*, *3*(3), 155–163.
- Bretthorst, G. L. (1988). *Bayesian spectrum analysis and parameter estimation*. New York: Springer-Verlag.
- Dalgaard, E., Auken, E., & Larsen, J. J. (2012). Adaptive noise cancelling of multichannel magnetic resonance sounding signals. *Geophysical Journal International*, *191*(1), 88–100.
- Davis, A. (2019). *Dipole surface nuclear magnetic resonance data for The Spot, WA*. v2. CSIRO. Data Collection. <https://doi.org/10.25919/5d48517c33564>
- Davis, A. C., Dlugosch, R., Queitsch, M., Macnae, J. C., Stolz, R., & Müller-Petke, M. (2014). First evidence of detecting surface nuclear magnetic resonance signals using a compact B-field sensor. *Geophysical Research Letters*, *41*, 4222–4229. <https://doi.org/10.1002/2014GL060150>
- Gregory, P. (2010). *Bayesian logical data analysis for the physical sciences: A comparative approach with Mathematica support*. Cambridge: Cambridge University Press. Paperback ed.
- Grombacher, D., Fiandaca, G., & Auken, E. (2019). Estimating T2 from surface NMR FID data using a forward model based on the full-Bloch equation. *Geophysical Journal International*, *218*(3), 1892–1902. <https://doi.org/10.1093/gji/ggz250>
- Hertrich, M., Green, A. G., Braun, M., & Yaramanci, U. (2009). High-resolution surface NMR tomography of shallow aquifers based on multioffset measurements. *Geophysics*, *74*(6), G47–G59.
- Irons, T. P., & Li, Y. (2014). Pulse and Fourier transform surface nuclear magnetic resonance: Comprehensive modelling and inversion incorporating complex data and static dephasing dynamics. *Geophysical Journal International*, *199*(3), 1372–1394. <https://doi.org/10.1093/gji/ggu323>
- Jiang, C., Müller-Petke, M., Lin, J., & Yaramanci, U. (2014). Magnetic resonance tomography using elongated transmitter and in-loop receiver arrays for time-efficient 2-D imaging of subsurface aquifer structures. *Geophysical Journal International*, *200*(2), 824–836.
- Lagarias, J. C., Reeds, J. A., Wright, M. H., & Wright, P. E. (1998). Convergence properties of the Nelder-Mead simplex method in low dimensions. *SIAM Journal of Optimization*, *9*, 112–147.
- Larsen, J. J., Dalgaard, E., & Auken, E. (2013). Noise cancelling of MRS signals combining model-based removal of powerline harmonics and multichannel Wiener filtering. *Geophysical Journal International*, *196*(2), 828–836.
- Legchenko, A., Comte, J.-C., Ofterdinger, U., Vouillamoz, J.-M., Lawson, F. M. A., & Walsh, J. (2017). Joint use of singular value decomposition and Monte-Carlo simulation for estimating uncertainty in surface NMR inversion. *Journal of Applied Geophysics*, *144*, 28–36.
- Müller-Petke, M., & Yaramanci, U. (2010). QT inversion—Comprehensive use of the complete surface NMR data set. *Geophysics*, *75*(4), WA199–WA209.
- Raiche, A., Sugeng, F., & Wilson, G. (2007). Practical 3D EM inversion? the P223f software suite, *ASEG extended abstracts* (Vol. 2007, pp. 1). Perth, Australia: CSIRO Publishing <https://doi.org/10.1071/ASEG2007ab114>
- Schirov, M., Legchenko, A., & Creer, G. (1991). A new direct non-invasive groundwater detection technology for Australia. *Exploration Geophysics*, *22*(2), 333–338. <https://doi.org/10.1071/EG991333>
- Shushakov, O. A. (1996). Groundwater NMR in conductive water. *Geophysics*, *61*(4), 998–1006. <https://doi.org/10.1190/1.1444048>
- Smith, A., Massuel, S., & Pollock, D. (2011). Geohydrology of the Tamala Limestone Formation in the Perth region: Origin and role of secondary porosity. Perth, Western Australia: CSIRO: Water for a Healthy Country National Research Flagship.
- Thébault, E., Finlay, C. C., Beggan, C. D., Alken, P., Aubert, J., Barrois, O., et al. (2015). International Geomagnetic Reference Field: The 12th generation. *Earth, Planets and Space*, *67*, 79.
- Vista Clara Inc. (2019). GMR-Vista Clara NMR Geophysics. Retrieved 2019-05-23 <http://www.vista-clara.com/products/surface-nmr/gmr/>
- Walbrecker, J. O., Hertrich, M., & Green, A. G. (2009). Accounting for relaxation processes during the pulse in surface NMR data. *Geophysics*, *74*(6), G27–G34.
- Walsh, D. O. (2008). Multi-channel surface NMR instrumentation and software for 1D/2D groundwater investigations. *Journal of Applied Geophysics*, *66*(3–4), 140–150.
- Weichman, P. B., Lavelly, E. M., & Ritzwoller, M. H. (2000). Theory of surface nuclear magnetic resonance with applications to geophysical imaging problems. *Physical Review E*, *62*(1), 1290–1312.